



City Research Online

City, University of London Institutional Repository

Citation: Read, M. (2024). A methodology for investigating the influence of hydrodynamic effects in gerotor type positive displacement machines. *Mechanism and Machine Theory*, 204, 105836. doi: 10.1016/j.mechmachtheory.2024.105836

This is the published version of the paper.

This version of the publication may differ from the final published version.

Permanent repository link: <https://openaccess.city.ac.uk/id/eprint/34048/>

Link to published version: <https://doi.org/10.1016/j.mechmachtheory.2024.105836>

Copyright: City Research Online aims to make research outputs of City, University of London available to a wider audience. Copyright and Moral Rights remain with the author(s) and/or copyright holders. URLs from City Research Online may be freely distributed and linked to.

Reuse: Copies of full items can be used for personal research or study, educational, or not-for-profit purposes without prior permission or charge. Provided that the authors, title and full bibliographic details are credited, a hyperlink and/or URL is given for the original metadata page and the content is not changed in any way.

City Research Online:

<http://openaccess.city.ac.uk/>

publications@city.ac.uk



Research paper

A methodology for investigating the influence of hydrodynamic effects in gerotor type positive displacement machines

Matthew Read

City, University of London, Northampton Square, London, EC1V 0HB, United Kingdom

ARTICLE INFO

Keywords:Gerotor
Oil pump
Hydrodynamic
Lubrication
Clearance

ABSTRACT

Positive displacement gerotor machines consisting of co-rotational and internally-meshed inner and outer rotors are widely used in liquid pumping applications. The necessary clearance gap between rotor profiles influences the contact behaviour and the internal leakage occurring between working chambers at different pressures. These depend on the dynamics of the idler rotor, which has not previously been investigated. This paper introduces a new approach to modelling the rotor dynamics, including the influence of hydrodynamic effects at the rotor contacts, bearing losses and the pumping torque. Epitrochoidal rotor profiles are used to investigate the influence of rotor geometry, clearances, and misalignment. The model provides insight into the effect of operating conditions, fluid properties, and material selection on the minimum film thickness achieved between the rotors, and the variation in clearance gap height. These results are essential for understanding how gerotor machines can be optimised to achieve high efficiency and a long operating life.

1. Introduction

Gerotor machines are compact and mechanically simple devices that are commonly used for a range of applications including oil and fuel pumps, and hydraulic motors. Numerous studies have explored the design and performance of gerotor machines. The rotor profiles used are critical in determining the resulting displacement and efficiency of the machine, and various mathematical methods for generating rotor profiles have been developed. Epitrochoidal and hypotrochoidal profiles are defined by a circular arc section for each lobe of one rotor, from which conjugate profiles for both rotors can be calculated [1–4]. Variations of basic epitrochoidal profiles have been described using non-circular generating arcs [5], and discrete curve sections to produce asymmetric profiles [6], while a novel alternative profile generation method based on deviation functions is described by Tong et al. [7]. Further aspects of profile geometry have been investigated, including identification of geometrical limits for valid trochoidal profiles [8–10], rotor contact behaviour [11,12], and the influence of clearances on rotor contact [13,14]. With the advent of advanced precision manufacturing methods, gerotor type profiles used with helical rotors have also received renewed interest for use in gas compression applications [15,16].

Key considerations for gerotor performance in liquid pumping applications relate to internal leakage, flow rate fluctuation, porting losses, and contact behaviour. Analysis and optimisation of rotor profiles and machine geometry have been performed using a variety of methods [17]. The influence of profile geometry on ideal volumetric capacity and flow rate fluctuations has been investigated [18]. The influence of rotor profile on wear in un-lubricated epitrochoidal and hypotrochoidal rotors has been explored using analytical and finite element methods [19,20], and the derived wear rate proportionality factor (WRPF) has been applied to optimise rotor profiles for minimum wear and flow irregularity [6,21]. Calculation of key geometrical characteristics relating to

E-mail address: m.read@city.ac.uk.

<https://doi.org/10.1016/j.mechmachtheory.2024.105836>

Received 1 July 2024; Received in revised form 21 September 2024; Accepted 1 November 2024

Available online 16 November 2024

0094-114X/© 2024 The Author.

Published by Elsevier Ltd.

This is an open access article under the CC BY license

(<http://creativecommons.org/licenses/by/4.0/>).

leakage, adhesive wear and Hertzian contact stresses has been used to perform multi-objective optimising, allowing the comparison of a range of profile types [22,23].

Gerotor pumps require high geometrical accuracy of the rotors to limit leakage flows and achieve the desired efficiency. While perfectly meshing conjugate rotors can be defined mathematically, a clearance must be applied to one or both rotor profiles to allow practical assembly and operation of the machines. In operation, internal fluid pressure generates radial bearing forces and net torques on each rotor [17]. In a typical pump application, the inner rotor is driven by an external power source, although a driven outer rotor is also possible. Power must then flow to or from the non-driven, or 'idler' rotor, to balance the net torque created by the fluid pressure, the influence of frictional losses in bearings and seals, and inertial effects. This transfer of power occurs via normal forces at the contact points.

The influence of rotor profile and clearance on the contact between rotors is crucial in understanding the operating cycle of the pump. Previous research has focussed on the following scenarios:

- For conjugate rotor profiles without clearance, operating in an un-lubricated machine, normal forces can be generated at all contact points where the applied torque causes the rotor faces to be pressed together; while the solution is indeterminate for rigid rotors, a solution can be found once the stiffness of the contacts is characterised [11,12,20].
- For a defined clearance applied to the profiles assuming un-lubricated rigid rotors, contact only occurs at a single point with clearance gaps present at all other 'nominal' contact points. With varying rotor position, if the clearance at one of these nominal contact points drops to zero, the contact will instantaneously jump to this new location. This variation in the single true contact point results in a periodic variation in transmission error [13]. For non-rigid rotors, the stiffness of the contacts can be used to find local deformations, which can lead to load sharing between more than one contact during the cycle [14].

No literature has been found addressing the scenario of lubricating liquid present between the rotors. In this case, the normal 'contact' forces are generated via hydrodynamic effects which occur simultaneously at all nominal contact points between the rotors. This scenario is representative of the actual operating conditions in a gerotor oil pump. The aim of the current study is not to provide a highly detailed and validated model of an actual pump, but to illustrate that hydrodynamic forces can have a significant influence on rotor dynamics. The key conclusion is that these effects should be included in future analytical models that aim to accurately capture variations in leakage path geometry and rotor wear.

The importance of understanding the contact behaviour of rotors in a gerotor pump is illustrated by Ranganathan et al. [24], in an experimental investigation of the relationship between wear, clearances and volumetric flow rate for a motorcycle oil pump application. This study explored the measured performance degradation over time, but does not consider the influence of geometry or operating conditions, which requires a more fundamental consideration of the pump design. A review of numerical analysis methods for gerotor and external gear pump machines [17] emphasises the importance of accurate clearance gap modelling for accurate prediction of performance, while noting that "the estimation of the real equilibrium position of the rotors represents a major breakthrough in the simulation of the gear pumps". There are several contributions in this area. Altare and Rundo [25] developed a 1D lumped-parameter model using a constant profile clearance model with an offset parameter to adjust the distribution of a constant clearance between minimum-volume and maximum-volume leakage paths; this was then tuned using experimental data covering a range of pressure, viscosity and rotational speeds. Gamez-Montero et al. [26] performed a CFD study to investigate the influence of profile clearance on volumetric flow rate using a fixed rotor and clearance geometry, with modification of viscosity used in the nominal contact patches to simulate the effect of zero clearance; rotational speed and pressure difference were shown to be important factors, and significant differences in flow rates were seen between cases with uniform clearances, no clearances, and no clearance at a single-point. Both studies illustrate the importance of understanding the relative rotor positions, but neither the lumped-parameter or CFD approaches consider the actual clearance geometry, hydrodynamics or contact mechanics.

A more fundamental study of the clearance geometry can be found in Demenego et al. [13] where a mathematically rigorous approach is used to characterise clearances at contacts between rigid rotors with circular pin-generated profiles, allowing the influence of profile clearance and rotor axis offset to be investigated. Gearing theory is applied to investigate transmission error assuming uni-directional power flow between rigid rotors, but there is no consideration of hydrodynamic effects, rotor deformation, or the influence of rotor inertia. Paffoni [12] describe an alternative clearance analysis method that uses small angle approximations; this is a more flexible approach that can estimate clearances for any defined rotor geometry. Contact points are assumed to be 'dry' (i.e. no fluid film present) and an estimated contact stiffness allows contact forces to be calculated for a given angular displacement with zero or non-zero [14] profile clearance. These 'dry' contact forces with non-zero clearance are used to estimate the required film thickness assuming elasto-hydrodynamic lubrication. There are a number of limitations to this approach; the film thickness is post-processed and does not feed back into the estimated rotor position, the hydrodynamic forces generated at other nominal contacts are neglected, and it does not consider the full range of possible lubrication regimes. Furthermore the calculation of film thickness is performed using the mean instantaneous velocity of the rotor surfaces tangential to the contact point; this is not appropriate for analysing gerotor contact point hydrodynamics, as discussed in more detail in Section 2.3. Pellegrini and Vacca [27] implement a different approach to identifying contact location by manipulating discretised rotor profile coordinates, and integrate this with a lumped parameter model for performance prediction. The model assumes single-point contact occurs with no rotor deformation, which depends of the direction of net torque on the idler rotor neglecting inertia. Hydrodynamics are considered for the journal bearing formed by the outer rotor and casing, but not in the rotor contact points.

In summary, there is a clear need for a rigorous method of predicting the influence of rotor geometry, material properties, and operating conditions on the rotor dynamics, as this is directly linked to machine efficiency and wear. This method must include consideration of the elasto-hydrodynamics in the nominal rotor contact patches. Furthermore, the influence of the idler rotor inertia on the motion has not previously been discussed in the literature, but must be included in the analysis due to the unsteady rotational speed of the idler that occurs even when the driven rotor speed is constant.

2. Methodology for analysing hydrodynamic effects in gerotor pumps

The purpose of the current study is to describe a methodology that has been developed to assess the influence of hydrodynamic effects on the relative motion of the rotors in an oil pump application. The novel analysis method has therefore been developed to achieve the following aims:

- Coupled investigation of surface deflection and elasto-hydrodynamic forces at all contact points.
- Rigorous analysis of outer rotor torsional dynamics, including influence of internal pressure forces, hydrodynamic forces, bearing drag losses and rotor inertia.
- Influence of rotor profile and axis offset on rotor dynamics, clearance gap height, film thickness and peak contact pressure.

A conventional approach to generating epitrochoidal profiles has been used throughout this paper. Definition of rotor geometry and contact conditions are discussed in Section 2.1. The contact geometry is influenced by the applied clearances and possible misalignment of rotor axis positions; since the clearance and rotor axis eccentricity must be small relative to rotor dimensions, a small angle approximation method is used to provide a simple analytical approach as described in Section 2.2. The generation of hydrodynamic forces in the contacts due to entrainment and film squeezing are characterised using a conventional Reynolds equation approach described in Section 2.3. The rotor dynamics analysis is described in Section 2.4, and details of the calculation procedure are provided in 2.5.

2.1. Epitrochoidal profile generation parameters

The subscripts 1 and 2 are used to denote the outer and inner rotors respectively. The dimensional parameters defining the rotor geometry are the inner rotor eccentricity, E , pin radius, r , and pin eccentricity, a . Two independent non-dimensional groups, λ and σ , can therefore be formed as shown in Eq. (1). This allows the shape of rotor profiles to be defined with three non-dimensional parameters; the number of lobes on the outer rotor, N_1 , the normalised pin radius, σ , and the normalised pin eccentricity, λ [16]. The rotor profile can then be sized by specifying either the maximum diameter of the outer rotor profile, D , or the inner rotor axis eccentricity, E . Once rotor profiles have been defined, the rotor-to-rotor contact points can be calculated as a function of the profile rotation angle, ϕ . The need to avoid undercutting of the inner rotor profile imposes a restriction on the maximum possible value of σ which is a function of N_1 and λ [8]. Hence a relative pin radius, $\bar{\sigma}$, can be defined as shown in Eq. (1); this is useful as it sets definite boundaries for the optimisation of profile and machine geometry. The parameters λ and $\bar{\sigma}$ characterise a consistent lobe shape across different values of N_1 .

$$\lambda = \frac{a}{N_1 E}, \quad \sigma = \frac{r}{N_1 E}, \quad \frac{E}{D} = \frac{1}{2N_1(\lambda - \sigma) + 4}, \quad \bar{\sigma} = \frac{\sigma}{\sigma_{\max}(N_1, \lambda)} \quad (1)$$

2.1.1. Geometry of contact points

The local curvature of the rotor surfaces is an important aspect of the contact mechanics. For an outer rotor profile with a non-conjugate root (shown in Fig. 1), the contact point on the outer rotor will always occur on the convex circular pin surface, while the contact on the inner rotor can occur at any point. The point at which the local surface curvature of the inner rotor passes through zero can be used to describe ‘tip’ and ‘root’ sections of the profile. It is then possible to determine whether a particular contact point is non-conformal (both inner and outer surfaces are convex) or conformal (inner surface is concave while outer is convex). This allows the contact point loci to be divided in conformal and non-conformal sections, as illustrated in Fig. 1. Conformal contact, hence low difference in surface curvature, is seen to occur when the contact point is close to the pitch point of the rotors. Furthermore, during the periods of conformal contact, the contact location is seen to move more rapidly along the surface of the rotors, which will influence the speed at which fluid is drawn into the contact patch. The conformal contact points are generally found to have more favourable conditions for hydrodynamic lubrication, which is discussed in more detail in Section 2.3. The angular position of the inner rotor where transition occurs between conformal and non-conformal contact is defined as $\phi_{2,lr}$, and is only a function of the profile geometry parameters N_1 and λ .

2.1.2. Torque exerted on rotors by fluid

The pressure of the working fluid during the pumping process will depend on leakage flows (a function of rotor geometry, clearance gaps, and operating conditions) and port design (which can be used to limit back flow rate and pressure pulsations, particularly if cavitation is occurring). Studies by Pellegrini et al. [28] and Altare and Rundo [25] have presented experimental measurements of discharge pressure variation compared against numerical results from lumped parameter models and 3D computational fluid dynamics. The fluctuations in pressure are shown to be relatively low at roughly $\pm 10\%$ in cases where there is little or no cavitation during the chamber filling process. In this study, a simple model is therefore used to estimate fluid pressure, which assumes that the suction and delivery pressures are constant, no pressure drops occur during filling or discharge, and pressure is uniform throughout a given working chamber. This is similar to the approach used by Paffoni et al. [14], and is a reasonable assumption for operation below the cavitation limit, allowing the key geometrical and operational parameters to be investigated without introducing a large number of additional factors. For a specified rotor geometry, the net torque per unit length exerted on the outer rotor by the fluid pressure in the working chambers, $M'_{1,pump}$, can be found as a function of the rotation angle by considering the location of contact points defining a particular working chamber [17]. Drag losses in the fluid film between the outer rotor and the casing can be approximated by the well known Petrov equation [29], which leads to a negative torque on the outer rotor as shown in Eq. (2). The diameter of the external surface of the outer rotor, D_o , should be kept as low as possible to minimise the drag losses, but needs

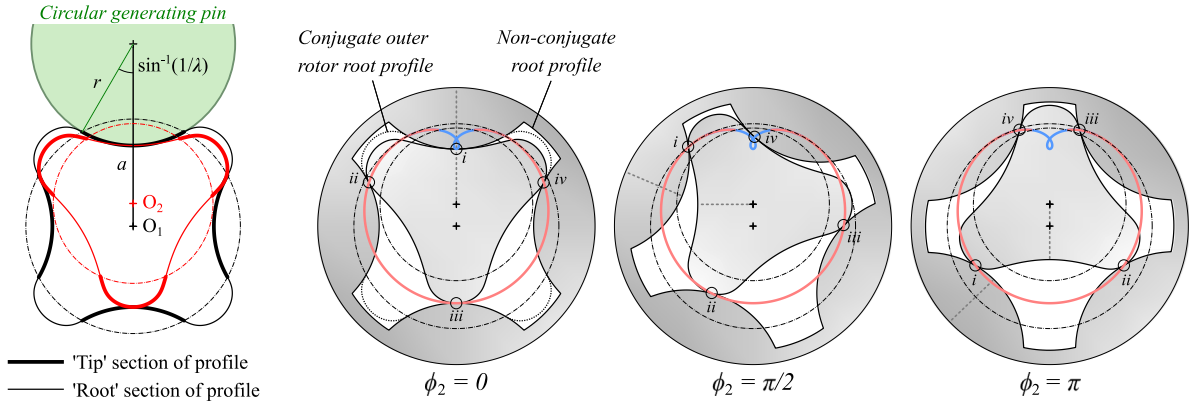


Fig. 1. Example illustrating the definition of rotor tip and root profile sections for case with $N_1 = 4, \lambda = 2, \bar{\sigma} = 0.8$, and the effect on the loci of the contact points when a non-conjugate outer rotor root profile is used.

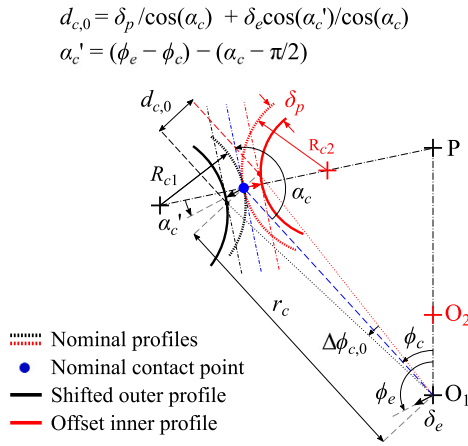


Fig. 2. Geometry of contact point with an offset inner rotor profile and a shifted outer rotor profile. Note that $d_{c,0}$ and hence $\Delta\phi_{c,0}$ are $-ve$ when $\alpha > \pi/2$ as shown.

to be large enough to maintain the strength and rigidity of the rotor. A value of $D_o = 1.1D$ is assumed for all cases presented in this paper. For the rotor-to-casing journal bearing clearance, $\delta_j = 100 \mu\text{m}$ has been used based on the range of values suggested by Gamez-Montero et al. [30].

$$M'_{1,drag} = \frac{M_{1,drag}}{L} = -\frac{\pi\eta_0\omega_1 D_o^3}{4\delta_j} \tag{2}$$

2.2. Rotor profile clearance geometry

The exact conjugate rotor profiles will be referred to here as the ‘nominal’ profiles to distinguish them from the more realistic profiles with clearance applied. The ‘nominal contact points’ are the locations where contact occurs with these nominal profiles; in general, gaps occur between the rotors at these points once clearance is applied. If the clearance is much smaller than the rotor diameter, the location of the nominal clearance points coincides with the minimum distance of approach between the rotor surfaces. A simple clearance distribution with constant normal offset applied to the nominal inner rotor profile is considered here. The outer rotor profile is unchanged, but the effect of shifting its rotational axis can also be investigated. This is of particular interest for gerotor pumps, where the outer rotor and casing form a hydrodynamic journal bearing; hence the speed and radial load applied to the outer rotor will affect the magnitude (δ_e) and direction (ϕ_e) of the rotor eccentricity relative to the centre of the nominal profile.

The resulting geometry at a nominal contact point is illustrated in Fig. 2, where:

1. α_c is the angle between the radial line connecting O_1 to the nominal contact point of the conjugate rotors, and the tangent to the profiles at the contact point.
2. The ‘profile clearance’, δ_p , is the offset distance normal to the original conjugate profile of rotor 2

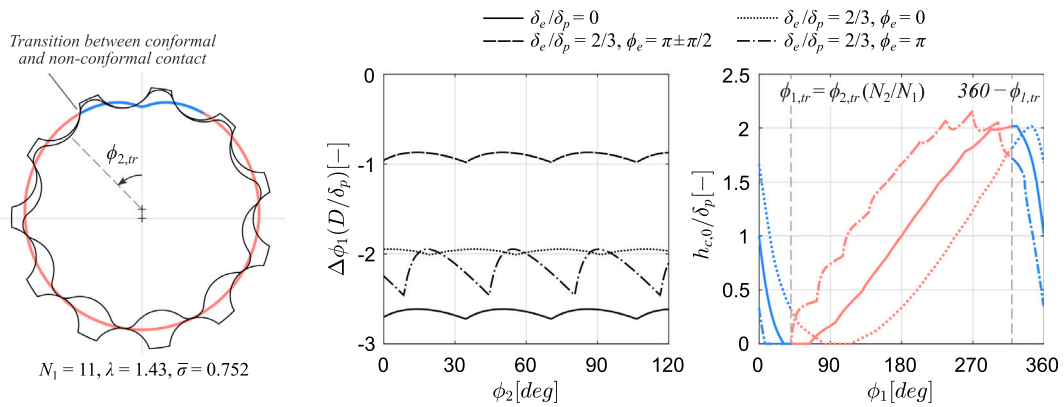


Fig. 3. Transmission error and backlash/gap height for contact with dry, rigid rotors and uni-directional power flow with driving inner rotor (for comparison with Demenego et al. 2002 where $D = 63.3$ mm and $\delta_p = 150$ μ m).

3. The ‘profile eccentricity’, δ_e , is the distance that the outer rotor profile is shifted by relative to the centre of the nominal rotor. This can occur due to clearances in the bearings for both rotors, in particular the outer hydrodynamic bearing where the clearance will vary with operating speed and load. To prevent interference between the rotor profiles, $\delta_e \leq \delta_p$.
4. $\Delta\phi_{c,0}$ is the angle that rotor 1 must rotate through in order to achieve contact with the offset profile of rotor 2, assuming rigid rotors. Applying the small angle approximation, $\Delta\phi_{c,0} \approx d_{c,0}/r_c$ which can be expressed as shown in Eq. (3).

$$\Delta\phi_{c,0} \approx \frac{\delta_p}{r_c} \left(\frac{1 + (\delta_e/\delta_p) \cos(\alpha'_c)}{\cos(\alpha_c)} \right) \quad (3)$$

The actual angular position of the outer rotor, ϕ_1^* , can be related to the actual angular offset of the outer rotor, $\Delta\phi^*$, and the inner rotor position as shown in Eq. (4).

$$\phi_1^* = \frac{N_2\phi_2}{N_1} + \Delta\phi^* \quad (4)$$

Once the value of $\Delta\phi^*$ is known, the normal height of the clearance gap at each nominal contact point assuming no rotor deformation can be calculated as shown in Eq. (5).

$$\frac{h_{c,0}}{\delta_p} \approx \frac{1}{\delta_p} (\Delta\phi_{c,0} - \Delta\phi^*) r_c \cos(\alpha_c) = 1 + \frac{\delta_e}{\delta_p} \cos(\alpha'_c) - \frac{r_c \Delta\phi^*}{\delta_p} \cos(\alpha_c) \quad (5)$$

The small angle approximation in Eq. (3) is valid while $d_{c,0} \ll r_c$. In cases where $\alpha_c \rightarrow \pm\pi/2$ (for example when the tips of the inner and outer rotors are in contact) it is apparent that $d_{c,0} \rightarrow \infty$. This is however not a problem, as the smallest value of $\Delta\phi_{c,0}$ occurring simultaneously at other contact points will limit the allowable offset rotation to a value in the order of $\pm\delta_p/D$. From Eq. (5) it can be seen that the calculated clearance height is only a function of this actual offset angle multiplied by $\cos(\alpha_c)$. Hence in cases where $\alpha_c = \pm\pi/2$, $\Delta\phi^*$ has no influence on the clearance gap, which is a good approximation if δ_p is much smaller than the local radius of curvature of both rotors. The method described therefore provides a good approximation to the clearance geometry when $\delta_p \ll \min(D, R_1, R_2)$. As the clearance gaps in gerotor pumps need to be several orders of magnitude smaller than the profile diameter in order to limit leakages, and the curvature at contact points should be limited to prevent high contact stresses, the small angle approximation method is considered suitable for these geometries; this is confirmed in the results shown in Fig. 3 which are indistinguishable from those presented by Demenego et al. [13], obtained using a more mathematically rigorous geometric method. The method described in this section is therefore used throughout the following analysis.

In Fig. 3, the misalignment of the outer rotor axis is seen to have a significant influence on the location of the single contact point (where $h_{c,0} = 0$) in dry, rigid rotors. Moving the outer rotor axis in the negative or positive y direction, the loci of this contact point moves towards or away from the conformal region respectively. Understanding the effect of this behaviour on the hydrodynamics of contact points, the dynamics of the outer rotor, and the leakage gap geometry, is a key motivation for the current study, and is discussed in detail in Section 3.5.

2.3. Hydrodynamic effects at nominal contact points

In oil-flooded applications, a fluid film forms in the nominal contact points, separating the rotor surfaces. This film is created by the combination of rolling and sliding motion at the surfaces drawing viscous fluid into the gap. In gerotor pumps, the entraining velocity, \bar{U} , at which oil is drawn into the contact point will depend on the instantaneous velocity of the rotor surfaces, but also the velocity of the contact zone itself as defined in Eq. (6) [29], where $v_{c1/2}$ is the component of the rotor surface velocity tangential to the contact point, and v_c is the tangential component of the contact patch velocity. Unlike dry (non-lubricated) applications which

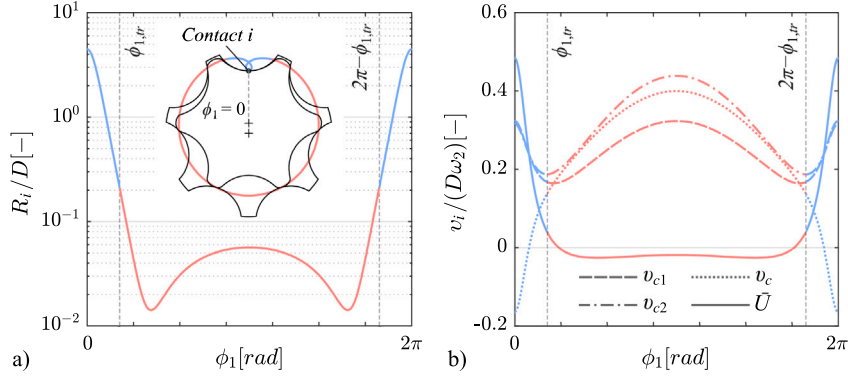


Fig. 4. Illustration of rotor profile described by Paffoni et al. [14], with the resulting normalised values of (a) reduced radius, and (b) contact velocities (v_{c1} , v_{c2} , v_c and \tilde{U}) shown for the evolution of contact point i with rotation angle. Loci of conformal and non-conformal contact are indicated by blue and red lines respectively. (For interpretation of the references to colour in this figure legend, the reader is referred to the web version of this article.)

rely on direct rotor-to-rotor contact to transmit forces, hydrodynamic forces are generated at all nominal contact points where there is a non-zero entraining velocity. The magnitude of this force per unit length, w' , depends on this entraining velocity, the reduced radius of curvature at the contact (R_c , defined in Eq. (7)), the clearance gap height (h_c), and the dynamic viscosity of the fluid (η).

$$\tilde{U}_c = \frac{1}{2} \left((v_{c1} - v_c) + (v_{c2} - v_c) \right) \quad (6)$$

$$\frac{1}{R_c} = \frac{1}{R_{c1}} + \frac{1}{R_{c2}} \quad (7)$$

Normalised values for the contact and entraining velocities and the reduced radius of curvature are presented in Fig. 4 for the rotor profile described by Paffoni et al. [14]. This illustrates the substantial difference between the tangential surface velocity of the rotors and the resulting entrainment velocity. For this rotor geometry, the magnitude of the entraining velocity is relatively low during the non-conformal contact between the tip sections of the inner and outer rotors, passing instantaneously through zero close to the transition angle. The reduced radius of curvature is also significantly lower during non-conformal contact. It is therefore apparent that the conformal contact locations generally have more favourable characteristics for achieving hydrodynamic lubrication with sufficient film thickness to prevent rotor contact and the resulting wear.

This hydrodynamic problem can be analysed using the Reynolds equation with the common assumptions of a Newtonian and incompressible fluid, laminar flow, smooth solid surfaces, and constant pressure through the film thickness. It is assumed that contact is infinitely long perpendicular to the flow direction, which allows the use of empirical relations to predict the hydrodynamic behaviour. The assumption is reasonable as the R_i/D value is shown to be generally small and L/D values in the range 0.5 – 2 is typical for practical gerotor pumps. End effects can become significant for hydrodynamic lubrication when $R_i/L > 0.5$, but for elasto-hydrodynamic lubrication values of R_i/L up to 5 have been shown to result in relatively low end effects in narrow bearings [31] and are in good agreement with the models described here. The Reynolds' equation is therefore applied in one dimension. Inertial and gravity effects are neglected and the gap height is considered small relative to the reduced radius. The boundary conditions used are no-slip conditions at rotor surfaces, and it is assumed that the pressure difference between far upstream and downstream locations is small relative to the peak hydrodynamic pressure. This is generally true for clearances between working chambers exposed to the same port where the pressure will be similar, although it may be less valid for clearances between chambers exposed to different ports when the pump is operating with high Δp . The approach used here is intended to investigate whether hydrodynamic forces have a significant influence on the motion of gerotor pump rotors, hence the simplifications described above are considered appropriate, but more detailed analysis considering the effects of finite line contact on hydrodynamic behaviour is recommended to provide an accurate model of rotor behaviour.

A non-dimensionalised film thickness parameter, h^* , is defined as shown in Eq. (8). The application of hydrodynamic bearing theory to the simple case of contact between rigid long cylindrical surfaces with constant fluid viscosity results in a value of $h^* = 4.89$ when the Reynolds boundary condition is applied. In cases where the deformation of the rotor surfaces becomes significant, the contact modulus (E^* , defined in Eq. (9)) is also required. Furthermore, under high pressure the viscosity of the fluid can change significantly as modelled using the Barus equation, which requires the pressure-viscosity index, α , to be specified along with the base viscosity, η_0 . Expressions for calculating h^* in the different regimes of rigid/elastic contact and constant/varying fluid viscosity are summarised in Table 1, with the non-dimensional parameters g_1 , g_3 and g_4 defined in Eq. (10). At a particular contact condition, the values of g_1 , g_3 and g_4 can be calculated and used with the equations in Table 1 to determine the relevant lubrication regime and to determine the corresponding film thickness.

$$h_c^* = \frac{w'_c h_c}{\eta_0 R_c \tilde{U}_c} \quad (8)$$

Table 1
Elasto-hydrodynamic regime boundaries and corresponding expression for film thickness parameter h^* [29].

Elasto-hydrodynamic regime:	Value of h^* :	Regime boundaries:
Rigid & isoviscous	4.89	–
Rigid & variable viscosity	$3.1g_3^{0.8}$	$h^* > 4.89, g_1 < 20, g_4 > 30$
Elastic & isoviscous	$g_1^{2/3}$	$h^* > 4.89, g_4 < 0.1$
Elastic & variable viscosity	$2.65g_1^{0.54}g_3^{0.06}$	$h^* > 4.89, 0.1 < g_4 < 100$

$$\frac{1}{E^*} = \frac{1 - \nu_1^2}{E_1} + \frac{1 - \nu_2^2}{E_2} \tag{9}$$

$$g_1 = \left(\frac{\alpha^2 (w'_c)^3}{\eta_0 R_c^2 \bar{U}_c} \right)^{1/2}, \quad g_3 = \left(\frac{(w'_c)^2}{2\eta_0 R_c \bar{U}_c E^*} \right)^{1/2}, \quad g_4 = \left(\frac{8\eta_0 \alpha^4 \bar{U}_c (E^*)^3}{R_c} \right)^{1/4} \tag{10}$$

The peak pressure occurring in the lubrication film is an important factor when considering wear in the rotors. When operating in the ‘rigid’ regimes the maximum fluid pressure can be calculated using the standard hydrodynamic analysis as shown in Eq. (11). In the ‘elastic’ regimes the pressure distribution is approximately Hertzian, allowing Eq. (12) to be used.

$$p_{\max} = 0.1988 \left(\frac{w'^3}{\eta \bar{U} R^2} \right)^{0.5} \text{ for ‘rigid’ lubrication regimes} \tag{11}$$

$$p_{\max} = p_0 = \left(\frac{E^* w'}{\pi R} \right)^{0.5} \text{ for ‘elastic’ lubrication regimes} \tag{12}$$

2.3.1. Elastic deformation at nominal contact points

If the load at a nominal contact point causes elastic deformation to occur, the relationship between rotor position and fluid film thickness is affected. If the rotors are considered to be rigid, the clearance gap height for a specified rotor offset angle is given by $h_{c,0}$ (Eq. (5)). For elastic rotors, however, any hydrodynamic force generated at this contact point will tend to deform the rotors such that this clearance gap increases. Schmid et al. [32] provide a detailed description of the Hertzian contact in rectangular conjunctions, such as between parallel cylinders, and derives the expression for the maximum deformation (i.e. the approach of centres) given in Eq. (13). This approach to calculating deformation is appropriate in the elasto-hydrodynamic lubrication regime, where the fluid pressure distribution is approximately Hertzian. The actual clearance gap height for the elastic rotor, h_c , is then given by Eq. (14).

$$\delta_{\max} = \frac{w'_c}{\pi E^*} \left[\ln \left(\frac{4\pi E^* R_c}{w'_c} \right) - 1 \right] \tag{13}$$

$$h_c = h_{c,0} + \delta_{\max} \tag{14}$$

For the rigid & isoviscous lubrication regime, the maximum fluid pressure is generally lower than the peak Hertzian pressure that would occur in a dry contact with the same load applied. Although deflection of the rotors can reasonably be neglected in this regime, it is important to avoid a discontinuity in the calculated value of δ_{\max} during transition between lubrication regimes, which is achieved using Eq. (15).

$$\frac{(\delta_{\max})_{\text{rigid}}}{(\delta_{\max})_{\text{elastic}}} = \frac{(h^*)_{\text{elastic}}}{(h^*)_{\text{rigid}}} = \left(\frac{2.65}{4.89} \right) g_1^{0.54} g_3^{0.06} \tag{15}$$

The calculation of hydrodynamic force and deformation are therefore coupled, and an iterative numerical approach is needed to find the solution for each nominal contact point with a given rotor offset angle $\Delta\phi^*$. The overall torque due to the hydrodynamic forces at all nominal contact points can then be assessed as shown in Eq. (16).

$$M'_{1,ehd} = - \sum_{c=1}^{N_1} w'_c r_c \cos(\alpha_c) \tag{16}$$

2.3.2. Squeeze film damping

In a gerotor pump, any angular motion of the idler rotor away from its nominal position will cause the surfaces of some contact points to move towards each other. The positive pressure generated by this squeezing of the fluid film creates a cushioning effect, with the damping force dependant on the contact geometry, the minimum film thickness, and the squeeze velocity ($v_{sq,c} = -dh_c/dt$). This hydrodynamic squeeze film damping must therefore be included in any analysis of rotor dynamics, but is difficult to assess for the complex geometry of the gerotor pump. A number of special cases are considered by Hamrock [33]; as a simplification, the approach taken here is to use the analytical solution for an infinitely long cylinder approaching a plane shown in Eq. (17), with a modification to the integration limits used to prevent unrealistically high forces when R_c becomes large relative to the rotor dimensions (Eq. (18)). The net torque applied on the outer rotor due to the squeeze film effect is then calculated as shown in Eq. (19).

$$\text{When } v_{sq,c} > 0, \quad w'_{sq,c} = \frac{6\eta_0 v_{sq,c} R_c}{h_c^2} (2R_c h_c)^{1/2} \int_{-\psi_{lim}}^{\psi_{lim}} \cos^2 \psi d\psi \tag{17}$$

$$\text{where } \psi_{lim} = \arctan\left(\frac{\min(R_c, D/(2N_1))}{(2R_c h_c)^{1/2}}\right) \quad (18)$$

$$M'_{1,sq} = - \sum_{c=1}^{N_1} w'_{sq,c} r_c \cos(\alpha_c) \quad (19)$$

2.4. Rotor dynamics

The torque required to overcome the fluid forces has been shown to vary with the angular position of the driven inner rotor, ϕ_2 . The hydrodynamic forces required at the nominal contact points, and the offset angle $\Delta\phi^*$ must also vary, resulting in non-zero angular acceleration of the outer rotor even when ω_2 is constant. The rotational inertia of the outer rotor is therefore an important factor, but has been neglected in all previous studies described in the literature. In reality, flexibility in the rotors, shafts and bearings mean that the rotors will be subject to forces leading to both lateral and torsional motion. In this study it is assumed that the lateral motion of the outer rotor is constrained by the fact that it rotates in a single continuous journal bearings with tight end face clearances [30]. The focus in this study is therefore purely on the torsional motion, although it is acknowledged that the influence of the journal bearing and end face film dynamics may need to be considered in future studies to fully understand the rotor motion. In the torsional equation of motion, the net torque per unit length that is exerted on the outer rotor is the sum of the hydrodynamic, squeeze film, oil drag, and bulk pumping torques, as shown in Eq. (20). The second moment of area of the outer rotor profile about the z -axis, J_1 , is used to find the outer rotor inertia, I_1 , for a given diameter of the outer surface, D_o , as shown in Eq. (21). As the inner rotor is generally driven by a primary source such as an engine or motor with significant additional inertia, it is reasonable to assume that the rate of change of inner rotor speed is zero.

$$I'_1 \frac{d^2 \phi_1^*}{dt^2} = M'_{1,net} = M'_{1,ehd} + M'_{1,sq} + M'_{1,drag} + M'_{1,pump} \quad (20)$$

$$\text{where } I'_1 = \frac{I_1}{L} = \rho_1 \left(\frac{\pi D_o^4}{32} - J_1 \right) \quad (21)$$

A numerical time-step based analysis is performed to solve this differential equation and find the offset angle of the outer rotor as a function of inner rotor angular position. The full calculation procedure is described in the following section.

2.5. Calculation procedure

The results presented in Sections 2.1 to 2.4 can be combined to analyse the influence of geometry and operating conditions on the rotor dynamics and contact mechanics of the gerotor pump. The various steps of the calculation procedure are illustrated in Fig. 5. The calculation procedure has been implemented in the Simulink environment using Matlab version 9.12.0.1884302 (R2022a), and allows the influence of a range of geometrical and operational parameters to be investigated, as discussed in detail in Section 3.

3. Case study

The influence on outer rotor dynamics of parameters including pressure difference, rotational speed, profile clearance, viscosity, and rotor eccentricity has been investigated using the profile described by Paffoni et al. [14] and illustrated in Fig. 4. Baseline parameter values for this case are given in Table 2. The inner rotor tip speed is chosen to be 50% of the maximum recommended by Gamez-Montero et al. [26] of 15 m/s, and a medium value of 15 bar pressure difference is used. The other geometry and fluid properties are chosen to match those used by Paffoni et al. [14]

3.1. Selection of calculation parameters

The simulation of the dynamic system describing the gerotor pump has been performed using a variable-step continuous numerical integration method to solve the ordinary differential equations. The fifth order Runge–Kutta–Dormand–Prince method (the 'ode45' solver in Simulink) is used in all cases presented here. A sensitivity analysis has been performed to identify appropriate values for two key parameters:

- The number of discrete steps for the angular position during generation of the rotor geometry, $n_{gen} = \pi/(N_2 \Delta\phi_2)$.
- The relative tolerance of the ode45 solver used in the rotor dynamics calculation.

The value of the minimum film thickness is highly sensitive to the calculation settings, and is used to assess the accuracy of the solution. The geometry generation parameter, n_{gen} , is increased until no significant variation in the calculated minimum film thickness is observed (Fig. 6). A value of $n_{gen} = 200$ combined with a relative tolerance of 10^{-8} can be seen to provide high accuracy with acceptable computation time for the analysis presented here. With the initial outer rotor offset angle set to zero and constant inner rotor speed, N_1 calculation cycles were found to achieve a converged operating cycle with a maximum relative error of 10^{-5} for consecutive minimum film thickness values. The total calculation time required to achieve a converged solution for a specified rotor geometry and operating condition is typically in the range of 50 – 100 s for the cases presented in the following section.

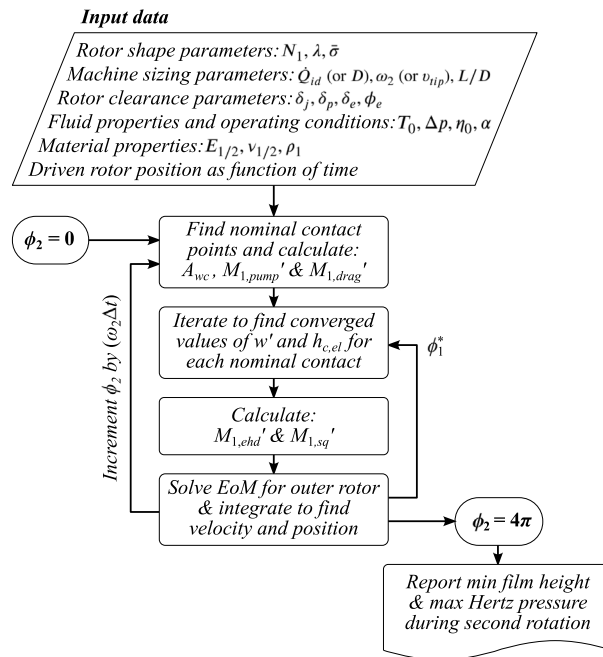


Fig. 5. Overview of the calculation procedure.

Table 2

Summary of parameter values for baseline case study. Note that material properties of steel are used for both rotors.

Baseline parameters	Value	Units
<i>Shape parameters:</i>		
N_1	7	–
λ	1.371	–
$\bar{\sigma}$	0.933	–
<i>Sizing parameters:</i>		
D	40.76	mm
v_{tip}	7.5	m/s
<i>Clearance parameters:</i>		
δ_j	100	μm
δ_p	50	μm
δ_e	0	μm
<i>Fluid parameters:</i>		
Δp	1.5	MPa
η_0	0.04	Pa s
α	$20e^{-9}$	Pa^{-1}
<i>Material parameters:</i>		
$E_{1/2}$	210	GPa
$\nu_{1/2}$	0.3	–
ρ_1	7850	kg/m^3

3.2. Case study results

Fig. 7 shows details of the converged solution for the outer rotor offset angle and the resulting relative gap height, film thickness and maximum fluid pressure. These results show that while the minimum clearance gap initially occurs at contact 'ii' when $0 < \phi N / (2\pi) < 0.3$, the combination of initially high \bar{U}_c and R_c at the conformal contact 'i' creates a large hydrodynamic force resulting in a positive angular acceleration of the outer rotor, lifting it clear of the inner rotor. The force generated at 'i' drops rapidly as $h_{c,i}$ increases; the constant drag torque and the increasing required fluid pumping torque cause the outer rotor to decelerate, while the squeeze film provides a cushioning effect as the rotor surfaces move together. The progressively less favourable hydrodynamic conditions at 'i' result in a small and decreasing value of $h_{c,i}$ until a minimum value is reached close to the point

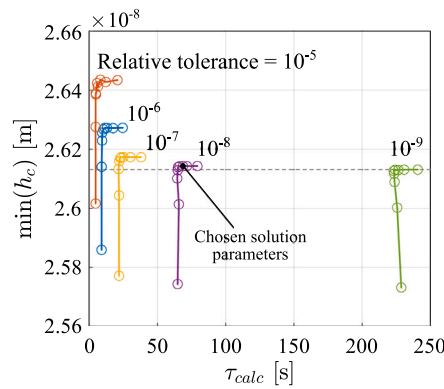


Fig. 6. Calculated minimum film thickness vs. total calculation time (τ_{calc}) for rotor geometry generation and solution of rotor dynamics for a complete rotation. Each curve shows results for a specified solver relative tolerance, and discrete rotation steps in the range $10 < n_{gen} < 1000$ during geometry generation. Baseline parameters are used as defined in Table 2.

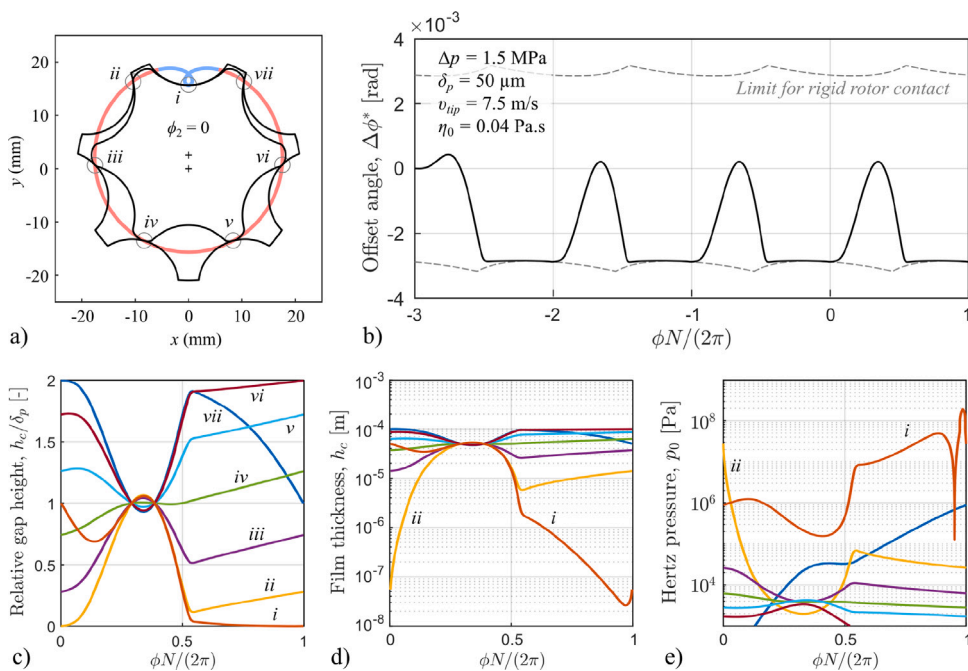


Fig. 7. Angular offset of outer rotor, relative gap height, film thickness and maximum pressure with the baseline conditions specified in Table 2.

where \bar{U} falls to zero (see Fig. 4). As no hydrodynamic force can be generated at this point, the fluid pressure falls rapidly, before increasing to a maximum value with non-conformal contact. The conformal contact point ‘vii’ can start to provide significant torque as ϕ increases beyond $2\pi/N$ and the cycle repeats.

3.3. Parametric study of outer rotor dynamics

The influence of four key parameters; operating pressure difference, rotational speed, fluid viscosity, and profile clearance, has been investigated by independently varying their values while keeping all other baseline parameters as defined in Table 2. The influence of fluid viscosity has been considered by assuming values of $\eta_0 = 0.01, 0.04$ and 0.29 Pa s, corresponding to SAE 15W-40 grade engine oil at temperatures of 20, 60 and 100°C . The results obtained in these cases are shown in Fig. 8, and illustrate that all key parameters can have a significant effect on the dynamics of the outer rotor. Motion of the outer rotor was found to be stable and cyclic with period of $\phi N / 2\pi\omega$ in all cases except at high tip speed where the motion repeats with period $\phi N / \pi\omega$.

In general, increasing Δp , decreasing η_0 , or increasing δ_p , is seen to reduce the amplitude of the fluctuations in $\Delta\phi^*$. Increasing speed leads to increased hydrodynamic forces and net torque which remains positive for a greater proportion of the cycle. The higher rotor acceleration acting for a shorter time results in similar maximum instantaneous velocity and amplitude of $\Delta\phi^*$ variation. The

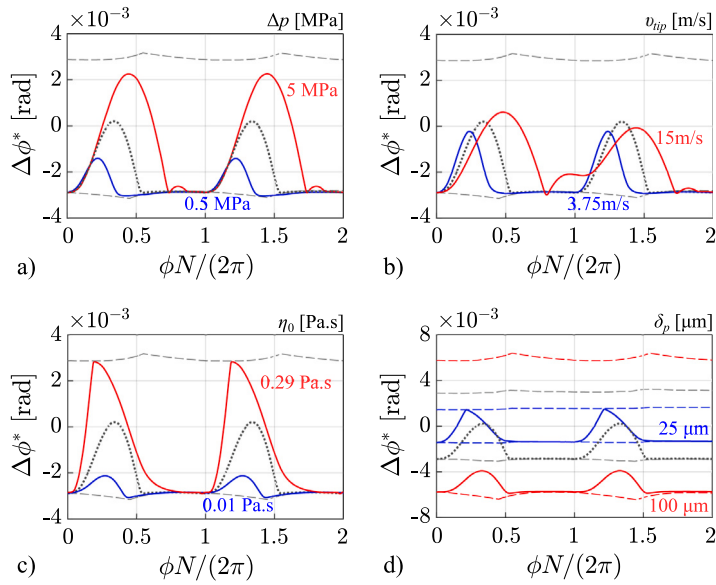


Fig. 8. Parametric study showing influence on outer rotor dynamics of independently varying (a) pressure difference, (b) inner rotor tip speed, (c) viscosity and (d) profile clearance, relative to the baseline conditions (grey dotted line, as shown in Fig. 7). (For interpretation of the references to colour in this figure legend, the reader is referred to the web version of this article.)

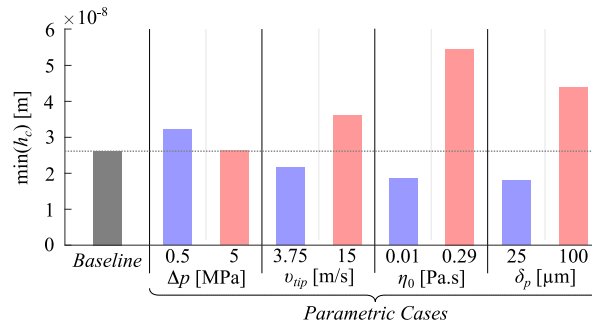


Fig. 9. Minimum film thickness for the cases shown in Fig. 8.

influence of δ_p on $\min(h_c)$ is less obvious; increasing the profile clearance causes the nominal contact where minimum film thickness occurs to dominate hydrodynamic torque generation, which may or may not be beneficial depending on the profile and operating conditions. Decreasing clearance can cause the outer rotor to ‘pinball’ between contacts at the positive and negative $\Delta\phi^*$ limits (as seen in Fig. 8d when $\delta_p = 25 \mu\text{m}$) leading to high accelerations and correspondingly low film thickness.

Fig. 9 shows the resulting minimum film thickness for the cases in Fig. 8. Reducing Δp , increasing v_{tip} and increasing η_0 , are all seen to increase the minimum film thickness, as might be expected from consideration of Eq. (8). It must be noted that the minimum film thickness predicted by EHL analysis must be considered relative to the surface roughness, as characterised by the ratio $\Lambda = \min(h_c)/R_a$. According to Dowson [34], hydrodynamic lubrication generally only occurs in gears when $\Lambda > 2$, while $\Lambda < 0.5$ results in significant asperity contact characteristic of the boundary lubrication regime. As steel with a ground finish has $R_a \approx 0.1 \mu\text{m}$, the results in Fig. 9 are in the range $0.2 < \Lambda < 0.6$. This baseline profile appears to suffer from a fundamental problem due to the requirement for rotor-to-rotor power transfer to occur with poor hydrodynamic conditions of low entraining velocity and low reduced radius at the nominal contact point with the lowest clearance; this is clearly seen when relating the baseline conditions in Fig. 7 to the nominal contact properties in Fig. 4. Changes in the operating conditions do not fundamentally change this contact behaviour, hence the consistently low values of minimum film thickness; it can be assumed that hydrodynamic lubrication would not occur under these conditions and an alternative analysis approach would be needed to accurately predict the actual behaviour. Operation of gerotor pumps in the hydrodynamic regime is however preferable to boundary or mixed regimes due to the lower friction and reduced wear. Hence the proposed analysis method is used to explore the rotor geometry and operating conditions necessary to achieve sufficient minimum film thickness, and where the assumptions of hydrodynamic lubrication are therefore appropriate.

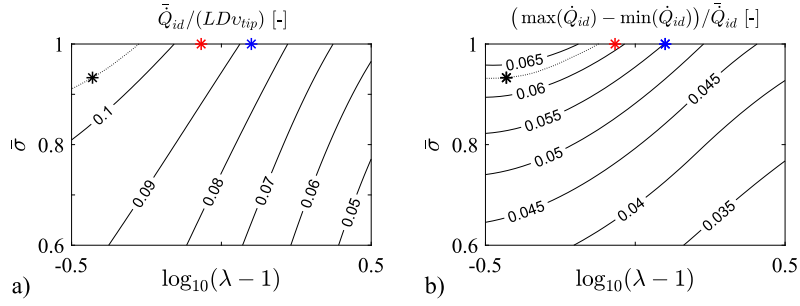


Fig. 10. Normalised values of (a) mean ideal volumetric flow rate, and (b) range of flow rate variation as a function of profile shape parameters for $N_1 = 7$. The black star represents the baseline profile, while the red and blue stars are referred to in Figs. 11 and 12. (For interpretation of the references to colour in this figure legend, the reader is referred to the web version of this article.)

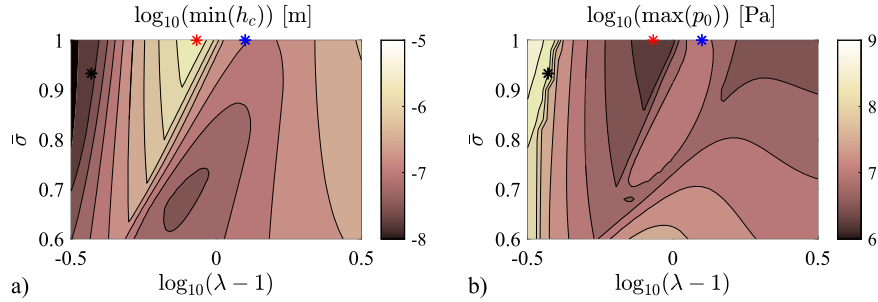


Fig. 11. Contour maps of (a) minimum film thickness and (b) maximum fluid pressure as a function of profile shape parameters for the baseline conditions in Table 2. The black star shows the baseline profile, while the red star shows the conditions with the largest minimum film thickness. (For interpretation of the references to colour in this figure legend, the reader is referred to the web version of this article.)

3.4. Influence of rotor profile

For a defined rotor geometry, the average and normalised range of the ideal volumetric flow rate, \bar{Q}_{id} , can be found as shown in Fig. 10. The influence of rotor profile on the hydrodynamics of the gerotor pump has been explored by calculating minimum film thickness and maximum fluid pressure for the baseline operating conditions, producing the results shown in Figs. 11. Relative to the baseline case, profiles with $1.5 < \lambda < 1.8$ and $\bar{\sigma} = 1$ achieve an increase in $\min(h_c)$ of 1–2 orders of magnitude and a corresponding reduction in maximum fluid pressure, with relative ideal flow rates of 100–94%. The influence of profile shape can be explored by considering that during the period $0 < \phi N / 2\pi < 1$ the conformal contact point i dominates the positive outer rotor torque contribution from hydrodynamic effects due to its comparatively high values of \bar{U}_c and R_c . A normalised torque available from this contact, M_i^* , can be defined as shown in Eq. (22), and is purely a function of the rotor profile shape parameters N_1 , λ and $\bar{\sigma}$.

$$M_i^* = \frac{M_i h_i}{\eta_0 \omega_2 L D^3 h^*} = - \left(\frac{R_i}{D} \right) \left(\frac{\bar{U}_i}{\omega_2 D} \right) \left(\frac{r_i \cos \alpha_i}{D} \right) \quad (22)$$

A comparison of the M_i^* values for three different rotor geometries is presented in Fig. 12 with the resulting outer rotor dynamics; the value of M_i^* provides a useful indication of the $\min(h_c)$ required to provide a given torque. The observed increase in minimum film thickness with some rotor geometries is a result of achieving a better match between M_i^* and the pumping torque required to drive the outer rotor (which is also geometry dependent), as illustrated in Fig. 13. In the optimal case ($\lambda_{opt} = 1.79$, $\bar{\sigma} = 1$), this leads to low acceleration of the outer rotor which limits the hydrodynamic loads, and results in high film thickness throughout the cycle. When $\lambda_{opt} < \lambda < 2.3$ the peak M_i^* value decreases more rapidly than the peak $M'_{1,pump}$ value, resulting in the observed decrease in minimum film thickness in this region.

3.5. Influence of rotor misalignment on film thickness

Misalignment of the rotors refers to an offset of the rotor axes relative to their nominal positions. There are two key factors relating to misalignment of the rotors:

1. The outer rotor forms a journal inside the casing bearing. The net force acting on the outer rotor will be largely due to the pressure difference across the machine and will act in the $+x$ direction for positive rotation. If the casing bearing surface is centred on the nominal axis, the outer rotor needs to move towards the $-\pi/2 < \phi_e < 0$ quadrant in order to generate

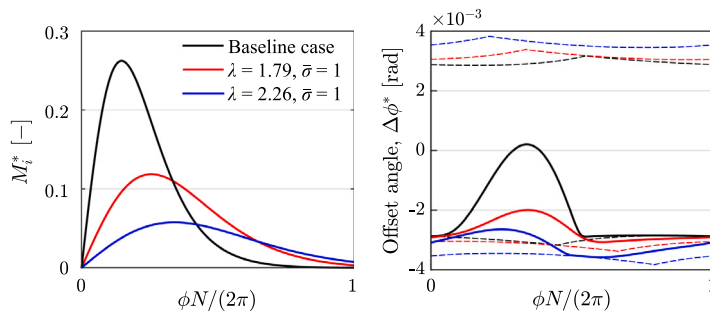


Fig. 12. The M_r^* characteristics and resulting outer rotor offset angles for the three geometries shown in Fig. 12; (i) the baseline case, (ii) the profile with largest minimum film thickness, and (iii) a higher λ case with reduced minimum film thickness.

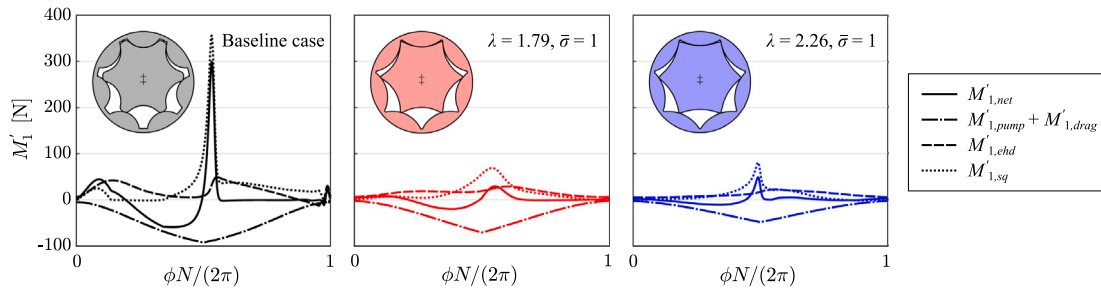


Fig. 13. Breakdown of outer rotor torque contribution for the three rotor geometries shown in Fig. 12.

the required hydrodynamic bearing force. The actual values of δ_e and ϕ_e will depend on the oil viscosity, journal bearing clearance, L/D ratio, rotor speed and load.

2. It has been suggested that the outer rotor should be deliberately offset in the $+y$ direction in order to reduce the leakage at the working chamber with maximum volume [30], where there is a high pressure difference and the non-conformal contact tends to increase leakage flow rate for a given clearance gap.

It is important to note that the clearances in an actual machine will depend on the bearings used and will be a function of speed and load. For a specific machine design, these factors can easily be introduced to the model to investigate how clearances and performance vary over a defined operating range. In the current study, we simply consider a range of relative offset distances between the rotor axes from zero to the maximum possible value of δ_p . If the inner rotor axis is assumed to be fixed, the outer rotor axis can be offset by a distance δ_e in direction ϕ_e (see Fig. 2). It is however more useful to consider a normalised offset in Cartesian coordinates as shown in Eq. (23).

$$\frac{1}{\delta_p} \begin{bmatrix} \Delta x_e \\ \Delta y_e \end{bmatrix} = \frac{\delta_e}{\delta_p} \begin{bmatrix} -\sin(\phi_e) \\ \cos(\phi_e) \end{bmatrix} \quad (23)$$

Relative to the case with no outer rotor offset ($\delta_e = 0$), movement in the positive or negative x direction is found to apply a constant shift to the offset angle of the outer rotor, $\Delta\phi^*$, but has no effect on the contact behaviour. Moving the outer rotor in the positive or negative y direction is however found to have a significant influence on the dynamics of the outer rotor. The results in Fig. 14 show how changes in Δy_e affect the minimum film thickness as a function of the rotor shape parameter λ for two values of pump pressure difference; assuming that both rotors are steel with surface roughness $R_a = 0.1 \mu\text{m}$, the dark and light grey regions indicate where $\Lambda < 0.5$ and $0.5 < \Lambda < 2$ respectively, corresponding to boundary and mixed lubrication regimes. The results in these regions should not be considered an accurate reflection of the real performance, as the assumptions used in the analysis are no longer valid. Above this upper limit of $\Lambda = 2$ however, the conditions are achieved for effective hydrodynamic lubrication of the surfaces. The change in $\min(h_c)$ with Δy_e is a result of changing the contact regions which dominate the hydrodynamic torque generation, as illustrated for specific cases in Fig. 15. Shifting the outer rotor in the $-y$ direction is found to enhance the contribution of the conformal contacts, generally allowing the required torque to be achieved with higher film thickness. A shift in the $+y$ direction leads to more reliance on torque generation from the non-conformal contacts closer to the maximum volume working chamber; the poor hydrodynamic conditions here tend to result in lower minimum film thickness and increased oscillations in offset angle.

An interesting result to note is that when operating with $\Delta p = 5 \text{ MPa}$, where the higher pressure difference causes an increase in the required pumping torque, it is only possible to achieve a practical minimum film thickness with $\Delta y_e/\delta_p < 0$. The results show that the movement of the outer rotor in the opposite direction due to bearing effects tends to impair the hydrodynamics at the rotor contacts. This can potentially be resolved by applying bearing preload; i.e. deliberately offsetting the centre of the casing bearing relative to the inner rotor shaft to achieve a specified offset in the $-y$ direction when operating at design conditions.

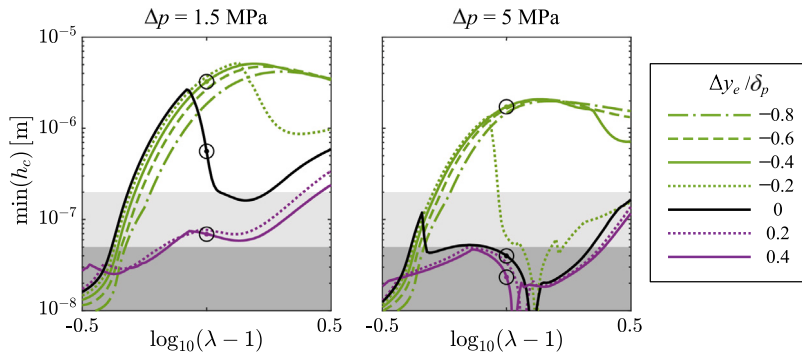


Fig. 14. Minimum film thickness calculated using baseline conditions with the specified values of Δp and $\Delta y_e/\delta_p$, and profiles with $\bar{\sigma} = 1$. The circled points have $\lambda = 2$ and correspond to the results shown in Fig. 15.

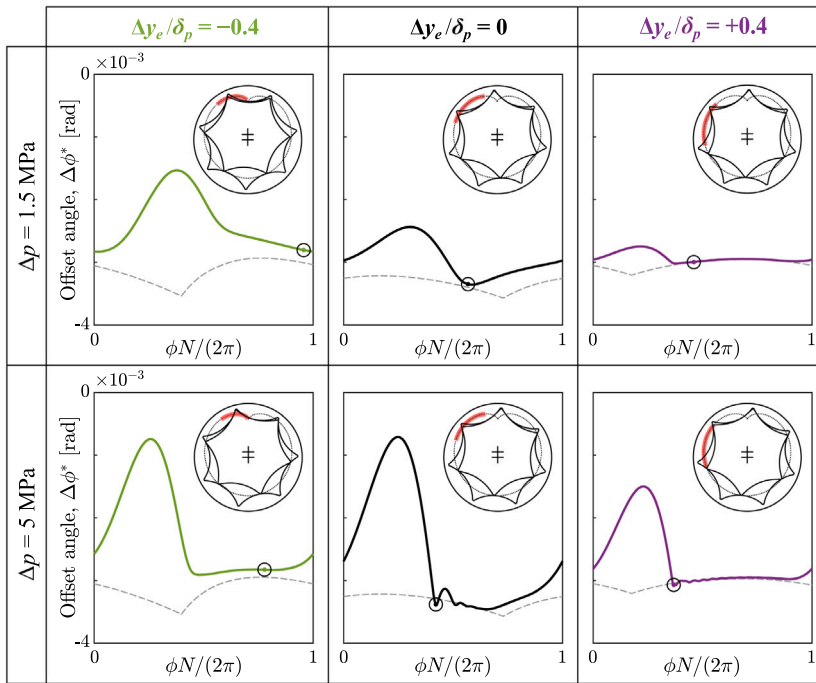


Fig. 15. Outer rotor offset angle and location of minimum film thickness for values of Δp and rotor misalignment shown in Fig. 14 with $\lambda = 2$ and $\bar{\sigma} = 1$. Rotors are shown in the position corresponding to overall minimum film thickness while red line shows the loci of instantaneous minimum film thickness. (For interpretation of the references to colour in this figure legend, the reader is referred to the web version of this article.)

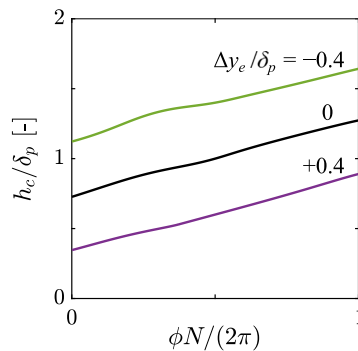


Fig. 16. Variation in clearance height for the maximum volume working chamber contact with large pressure difference, when using baseline conditions with $\lambda = 2$, $\bar{\sigma} = 1$ and the specified outer rotor misalignment.

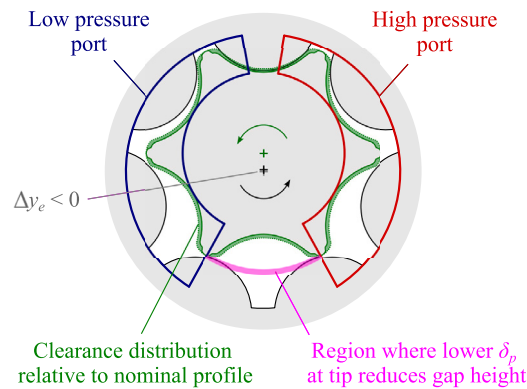


Fig. 17. Example of varying profile clearance to limit leakage flow across the maximum volume contact point separating high and low pressure ports, while still achieving the hydrodynamic benefits of negative Δy_e . Note that the scale of the clearance distribution has been exaggerated for clarity.

The results in Fig. 16 show that, as expected, shifting the outer rotor in the $+y$ direction can significantly reduce the leakage height at the key contact point in the maximum volume working chamber which experiences a high pressure difference. This is however likely to have a negative impact on rotor wear due to the associated decrease in film thickness; the leakage gap should be limited by choosing the highest value of $\Delta y_e / \delta_p$ that provides adequate film thickness for the required operating conditions. It should, however, be noted that this study has only considered the effect of a constant profile clearance. The clearance can, in principle, be varied along the rotor profile. This is illustrated in Fig. 17 using an exaggerated scale for the clearances; by reducing the clearance around the inner rotor tip, the leakage gap height can be reduced in the maximum volume region, while allowing the benefits of high film thickness associated with $\Delta y_e \geq 0$.

It is clear that designs incorporating bearing preload and/or variable profile clearance will need detailed knowledge of the application and operating requirements of the pump, as well as the manufacturing requirements of the rotors. While optimisation of both leakage and hydrodynamic lubrication is possible, the duty cycle of the pump and the requirements for off-design operation will need careful consideration to achieve effective management of efficiency and rotor wear.

4. Conclusions

While there is extensive literature relating to geometrical analysis and performance prediction for gerotor pumps, there has been limited previous focus on the dynamic behaviour of gerotor pump rotors, or the hydrodynamics of the rotor-to-rotor contacts. A modelling approach has therefore been proposed and demonstrated across a range of conditions. The minimum film thickness and maximum fluid pressure are found to be highly dependent on rotor geometry, axis alignment, fluid properties and operating conditions, all of which can be investigated with the current model. This approach is key to developing a fundamental understanding of both mechanical wear and the nature of the interlobe leakage channels. The main conclusions of the current study can be summarised as follows:

- Hydrodynamic conditions are found to be relatively good at conformal contact points, where entraining velocity and reduced radius are both generally high. These properties are lower in the non-conformal contact region, impairing the ability to generate hydrodynamic forces.
- Overall minimum film thickness an order of magnitude greater than the surface roughness of ground steel has been predicted for typical operating conditions when using optimised rotor geometry with a value of $\bar{\sigma} = 1$ (i.e. the maximum generating pin radius possible without undercutting). Relative to a baseline profile, a significant increase in minimum film thickness was possible with no reduction in ideal volumetric flowrate.
- Misalignment of the outer rotor in the y direction is found to strongly influence the contact hydrodynamics, affecting both the minimum film thickness and the region in which this occurs;
 - $\Delta y_e < 0$ moves the loci of instantaneous $\min(h_c)$ towards the conformal contact region, generally enhancing the hydrodynamic performance and increasing the minimum film thickness.
 - $\Delta y_e > 0$ moves the loci away from the conformal contact region, generally degrading hydrodynamic performance and reducing the overall minimum film thickness.
- Applying preload to the outer rotor journal bearing, and a varying rotor clearance distribution have been identified as possible ways of optimising both film thickness and leakage flows.

The main contribution of this study is the finding that rotor dynamics are an essential element in understanding the leakage and wear characteristics of gerotor pumps for a particular application. Another contribution of this research is the ability to use the proposed model to provide a rigorous method of specifying appropriate values of leakage gap height depending on machine geometry and operating conditions, which is necessary for accurate performance prediction. The current study applies a number of

simplifications, and more detailed analysis of rotor dynamics including the lateral as well as torsional behaviour is an important area for future work. This would allow a detailed theoretical investigation of the influence of clearance geometry, rotor misalignment, material selection and contact hydrodynamics, which will require rigorous experimental validation. The development of accurate rotor dynamics and machine performance models will allow designers to identify optimum strategies aimed at improving volumetric efficiency without impairing the lifespan and long-term performance of the machine.

Declaration of competing interest

The authors declare that they have no known competing financial interests or personal relationships that could have appeared to influence the work reported in this paper.

Acknowledgement

Funding for this research was received from Carrier Global Corporation, USA and PDM Analysis Ltd., UK.

Data availability

Data will be made available on request.

References

- [1] J. Colbourne, The geometry of trochoid envelopes and their application in rotary pumps, *Mech. Mach. Theory* 9 (3–4) (1974) 421–435.
- [2] J.E. Beard, A.S. Hall, W. Soedel, Comparison of hypotrochoidal and epitrochoidal gerotors, *J. Mech. Des.* 113 (2) (1991) 133–141.
- [3] J. Beard, D. Yannitell, G. Pennock, The effects of the generating pin size and placement on the curvature and displacement of epitrochoidal gerotors, *Mech. Mach. Theory* 27 (4) (1992) 373–389.
- [4] J. Shung, G. Pennock, Geometry for trochoidal-type machines with conjugate envelopes, *Mech. Mach. Theory* 29 (1) (1994) 25–42.
- [5] G. Mimmi, P. Pennacchi, Rotor design and optimization in internal lobe pumps, *Appl. Mech. Rev.* 50 (11S) (1997) S133–S141.
- [6] G. Jacazio, A. De Martin, Influence of rotor profile geometry on the performance of an original low-pressure gerotor pump, *Mech. Mach. Theory* 100 (2016) 296–312.
- [7] S.H. Tong, J. Yan, D.C. Yang, Design of deviation-function based gerotors, *Mech. Mach. Theory* 44 (8) (2009) 1595–1606.
- [8] D. Vecchiato, A. Demenego, J. Argyris, F.L. Litvin, Geometry of a cycloidal pump, *Comput. Methods Appl. Mech. Engrg.* 190 (18–19) (2001) 2309–2330.
- [9] Y.W. Hwang, C.F. Hsieh, Geometric design using hypotrochoid and nonundercutting conditions for an internal cycloidal gear, *J. Mech. Des.* 129 (4) (2006) 413–420.
- [10] S.M. Kwon, H.S. Kang, J.H. Shin, Rotor profile design in a hypogerotor pump, *J. Mech. Sci. Technol.* 23 (2009) 3459–3470.
- [11] J.B. Shung, G.R. Pennock, The direct contact problem in a trochoidal-type machine, *Mech. Mach. Theory* 29 (5) (1994) 673–689.
- [12] B. Paffoni, Pressure and film thickness in a trochoidal hydrostatic gear pump, *Proc. Inst. Mech. Eng. G* 217 (4) (2003) 179–187.
- [13] A. Demenego, D. Vecchiato, F.L. Litvin, N. Nervegna, S. Mancó, Design and simulation of meshing of a cycloidal pump, *Mech. Mach. Theory* 37 (3) (2002) 311–332.
- [14] B. Paffoni, R. Progri, R. Gras, Teeth clearance effects upon pressure and film thickness in a trochoidal hydrostatic gear pump, *Proc. Inst. Mech. Eng. G* 218 (4) (2004) 247–256.
- [15] W. Hu, Z. He, D. Li, K. Ma, Z. Xing, Geometry of intersecting-axis conical twin-screw rotors, *Mech. Mach. Theory* 174 (2022) 104913.
- [16] M.G. Read, N. Stosic, I.K. Smith, The influence of rotor geometry on power transfer between rotors in gerotor-type screw compressors, *J. Mech. Des.* 142 (7) (2020) 073501.
- [17] M. Rundo, Models for flow rate simulation in gear pumps: A review, *Energies* 10 (9) (2017) 1261.
- [18] G. Bonandrini, G. Mimmi, C. Rottenbacher, Theoretical analysis of internal epitrochoidal and hypotrochoidal machines, *Proc. Inst. Mech. Eng. C* 223 (6) (2009) 1469–1480.
- [19] P. Yun, H. Nam, C. Kim, J.H. Shin, S.M. Kwon, Optimal wear design for a gerotor pump using genetic algorithm, in: 2010 IEEE International Conference on Mechatronics and Automation, IEEE, 2010, pp. 207–212.
- [20] S.M. Kwon, C.H. Kim, J.H. Shin, Optimal rotor wear design in hypotrochoidal gear pump using genetic algorithm, *J. Cent. South Univ.* 18 (2011) 718–725.
- [21] M. Karamooz Ravari, M. Forouzan, H. Moosavi, Flow irregularity and wear optimization in epitrochoidal gerotor pumps, *Meccanica* 47 (2012) 917–928.
- [22] A. Robison, A. Vacca, Multi-objective optimization of circular-toothed gerotors for kinematics and wear by genetic algorithm, *Mech. Mach. Theory* 128 (2018) 150–168.
- [23] A.J. Robison, A. Vacca, Performance comparison of epitrochoidal, hypotrochoidal, and cycloidal gerotor gear profiles, *Mech. Mach. Theory* 158 (2021) 104228.
- [24] G. Ranganathan, T.H.S. Raj, P.M. Ram, Wear characterisation of small PM rotors and oil pump bearings, *Tribol. Int.* 37 (1) (2004) 1–9.
- [25] G. Altare, M. Rundo, Advances in simulation of gerotor pumps: An integrated approach, *Proc. Inst. Mech. Eng. C* 231 (7) (2017) 1221–1236.
- [26] P.J. Gamez-Montero, R. Castilla, D. del Campo, N. Ertürk, G. Raush, E. Codina, Influence of the interteeth clearances on the flow ripple in a gerotor pump for engine lubrication, *Proc. Inst. Mech. Eng. D* 226 (7) (2012) 930–942.
- [27] M. Pellegri, A. Vacca, Numerical simulation of gerotor pumps considering rotor micro-motions, *Meccanica* 52 (8) (2017) 1851–1870.
- [28] M. Pellegri, A. Vacca, E. Frosina, D. Buono, A. Senatore, Numerical analysis and experimental validation of gerotor pumps: A comparison between a lumped parameter and a computational fluid dynamics-based approach, *Proc. Inst. Mech. Eng. C* 231 (23) (2017) 4413–4430, <http://dx.doi.org/10.1177/0954406216666874>.
- [29] J.A. Williams, *Engineering Tribology*, Cambridge University Press, 2005.
- [30] P.J. Gamez-Montero, R. Castilla, E. Codina, Methodology based on best practice rules to design a new-born trochoidal gear pump, *Proc. Inst. Mech. Eng. C* 232 (6) (2018) 1057–1068.
- [31] M. Zhang, J. Wang, J. Cui, P. Yang, A thermal EHL investigation on plate-pin hinge pairs in silent chains using a narrow finite line contact, *Ind. Lubr. Tribol.* 72 (10) (2020) 1139–1145.
- [32] S.R. Schmid, B.J. Hamrock, B.O. Jacobson, *Fundamentals of Machine Elements*, CRC Press, 2013.
- [33] B.J. Hamrock, *Fundamentals of fluid lubrication*, vol. 1255, National Aeronautics and Space Administration, Scientific and Technical Information Program, 1991.
- [34] D. Dowson, Elastohydrodynamic and micro-elastohydrodynamic lubrication, *Wear* 190 (2) (1995) 125–138.